RSC Advances

PAPER

View Article Online
View Journal | View Issue

Cite this: *RSC Adv.*, 2021, **11**, 12520

All carbon hybrid N-doped carbon dots/carbon nanotube structures as an efficient catalyst for the oxygen reduction reaction†

Anh Thi Nguyet Nguyen and Jun Ho Shim *

This paper reports the facile and scalable synthesis of hybrid N-doped carbon quantum dots/multi-walled carbon nanotube (CD/CNT) composites, which are efficient alternative catalysts for the oxygen reduction reaction (ORR) in fuel cells. The N-doped CDs for large-scale production were obtained within 5 minutes *via* a one-step polyol process using ethylenediamine (ED) in the presence of hydrogen peroxide as an oxidizing agent. For comparison, different CDs were also prepared using ethylene glycol (EG) and ethanolamine (EA) in the same manner. Physicochemical characterization suggested the successful formation of a CD(ED)/CNT hybrid without individual CD(ED)s and CNTs. The N-doped CD(ED)/CNT catalyst exhibited excellent electrocatalytic activity in an alkaline solution compared to other composites (CD(EG)/CNT and CD(EA)/CNT). The Tafel slope (−60.9 mV dec^{-1}) and durability (~9.1% decay over 10 h) for CD(ED)/CNT were superior to high-performance Pt/C catalysts. The electrochemical double-layer capacitance on the CD(ED)/CNT hybrid showed apparent improvement of the active surface area because of N-doping and highly decorated CDs on the CNT wall. These results provide an innovative approach for the potential application of all carbon hybrid structures in electrocatalysis.

Received 13th February 2021
Accepted 25th March 2021

DOI: 10.1039/d1ra01197a

rsc.li/rsc-advances

Introduction

The demand for competitive alternatives to precious platinum as highly active oxygen reduction reaction (ORR) electrocatalysts has increased because the commercial applications of Pt-based catalysts are limited by their high cost, CO deactivation, and poor durability.[1–3] Several strategies have been explored to replace commercial Pt-based catalysts with metal-free carbon materials. Metal-free-based catalysts possess desirable properties such as high electrical conductivity, high surface area and relatively good stability.[4–6] In addition, they are inexpensive, environmentally friendly, and durable in acid and alkaline media.[4–7] Moreover, carbon materials modified by heteroatom doping (such as boron (B),[8,9] phosphorous (P),[10–12] nitrogen (N),[13–19] and sulfur (S)[20–23]) show the improved electrocatalytic activity of carbon-based materials. This is because the embedded heteroatoms can alter the local spin or charge density considerably by producing an irregular charge distribution in the adjacent sites, thereby enhancing the electronic conductivity and promoting adsorption and activation of molecular oxygen.[24,25]

In the carbon material family, carbon quantum dots (CQDs, C-dots, or CDs) as a new class of zero-dimensional nanocarbon with sizes below 10 nm, showed good solubility, low cytotoxicity, great compatibility, and simple synthesis, and could be functionalized with surface passivation.[26,27] CDs have highly defective oxygen-containing moieties that are distributed randomly at the basal plane and edge sites. Moreover, CDs have been widely employed in solar cells,[28] electrochemical capacitors,[29] optoelectronic devices,[30] drug delivery,[31] fluorescent bioimaging,[32] and sensors[33] because of their strong quantum confinement and edge effects. Unfortunately, the applications of CDs in oxygen-involving reactions are limited by their poor electrical conductivity. In addition, CDs tend to aggregate, which restricted the exposure of the active sites and electron transfer.[34] Accordingly, great developments have been made to enhance their dispersion and electrocatalytic activity by decorating CDs on a conductive substrate, such as graphene,[24,35–38] graphene nanoribbons,[39] and multi-walled carbon nanotubes.[40,41]

J. Zhang *et al.*[40] synthesized nitrogen-doped carbon quantum dots/multiwall-carbon nanotube-supported Pt (Pt/NCQD–MWCNT), which exhibited 1.3 times higher activity for methanol electrooxidation than Pt/MWCNT, highlighting the enhanced catalytic activity with the addition of NCQDs. Nevertheless, this hybrid material has not been used as an ORR electrocatalyst. The presence of noble-metal Pt remains a challenge to develop metal-free catalysts with high activity, low cost, and strong durability that can be produced under mild conditions. X. Zhou *et al.*[41] reported that a novel metal-free electrode composed of graphene quantum dots (GQDs) and MWCNT enhanced the electrocatalytic activity toward the ORR, improved

Department of Chemistry and Institute of Basic Science, Daegu University, Gyeongsan 38453, Republic of Korea. E-mail: junhoshim@daegu.ac.kr

† Electronic supplementary information (ESI) available. See DOI: 10.1039/d1ra01197a

long-term durability, and showed excellent resistance to the crossover effect compared to commercially available Pt/C catalysts. On the other hand, the ORR performance of this composite is still low. Furthermore, carbon quantum dots synthesis is a time-consuming process. Thus far, the effects of different CQDs precursors have not been studied systematically.

Over the past few decades, studies of the structure, properties, and applications of one-dimensional (1D) multi-walled carbon nanotubes (CNTs) have been a hot topic in nanotechnology, particularly in electrochemical fields because of their superior electrical conductivity, high chemical stability, and large surface area. On the other hand, the inherent inertness of the CNT wall is a significant challenge in depositing particles uniformly over the surface of CNTs. Therefore, CNT surfaces need to be modified to improve the dispersibility of nanoparticles. According to an excellent review,[42] the decoration of CNTs can be carried out directly on the CNT surface or connecting particles with CNTs by (a) covalent linkage, (b) hydrophobic interactions and hydrogen bonds, (c) π-stacking, and (d) electrostatic interactions. Many studies have reported that functionalized CNTs decorated with metal atoms can be a good candidate for energy storage systems.[43–46] On the other hand, only a few achievements for the decoration of CNTs using CDs as precursors have been reported because of the semiconductivity of CDs.

In this study, a novel metal-free defect-rich carbon quantum dots/multi-walled carbon nanotubes (CD/CNT) composite was developed as a highly efficient alternative catalyst for ORR using a facile refluxing approach. N-doped CDs for large-scale production were obtained using a simple one-step polyol process within 5 minutes using ethylenediamine (ED) in the presence of H_2O_2 as an oxidizing agent. For comparison, different CDs were also prepared using ethylene glycol (EG) and ethanolamine (EA) in the same manner. Highly N-doped CDs provide more active edges and defect sites. CNTs, which act as a conducting substrate, may facilitate electron transfer and prevent the aggregation of CDs to expose more active sites for the ORR. The achieved CD(ED)/CNT composite showed improved electrocatalytic activity and good durability in alkaline solutions compared to other composites. The effects of different CD precursors on the catalytic performance of CD/CNTs, such as CD(EG)/CNT and CD(EA)/CNT catalysts, were also investigated.

Experimental

Chemicals and characterizations

Ethylene glycol (EG), ethanolamine (EA), ethylenediamine (ED), multi-walled carbon nanotubes (CNTs), and hydrogen peroxide (28%, H_2O_2) were supplied by Duksan Co. (Korea). Commercial Pt/C catalysts (20 wt% Pt loading) was a product of E-TEK. The aqueous solutions were prepared with deionized water. The morphologies of all synthesized samples were observed by transmission electron microscopy (TEM, Philips, CM-200). The Fourier-transform infrared (FTIR) spectra of the samples were recorded on a Thermo Fisher Scientific Nicolet iS5 FTIR spectrometer. The UV-Vis absorption spectra (Shimadzu UV-1900I) were collected over the wavelength range of 200 nm to 500 nm. The photoluminescent (PL) spectra were examined by a PicoQuant FluoTime 200 Compact Fluorescence Spectrometer. The Raman spectra were recorded on a model XploRa plus (HORIBA) Raman spectrometer (laser excitation at 532 nm). The surface properties of the catalysts were analyzed by X-ray photoelectron spectroscopy (XPS, AXIS Nova) using Al Kα monochromatized radiation.

Synthesis of carbon dots

The carbon quantum dots (CDs) were synthesized from three different carbon sources (EG, EA, and ED, respectively) using a facile one-step polyol process. First, 10 mL of H_2O_2 was added to a 250 mL beaker containing 10 mL of EG. The mixture was placed in a stove at 250 °C and kept for 10 minutes. During this time, the colorless solution changed to a yellow CD colloid. The products are denoted as CD(EG). In the same way, N-doped CDs were prepared from EA and ED precursors, respectively, and called CD(EA) and CD(ED), respectively. Hydrogen peroxide (10 mL) was added dropwise to a 250 mL beaker containing 10 mL of EA. The color of the amine precursor turned orange, and air bubbles were generated immediately after H_2O_2 was added. The mixture was placed on a stove at 250 °C and kept for 7 min until a dark brown CD(EA) colloid formed. CD(ED) was also prepared from an ED precursor. For the synthesis of the CD(ED) precursor, 10 mL of H_2O_2 was added dropwise to a 250 mL beaker containing 10 mL of ED. The color of the amine precursor turned dark yellow, and air bubbles were generated immediately after the H_2O_2 was added. The mixture was placed on a stove at 250 °C and kept for 5 min until a dark brown CD(ED) colloid formed. All obtained CD colloidal products were washed using a dialysis membrane for 24 h, and dissolved quickly in deionized water. A homogeneous suspension of CDs was stored in the dark at room temperature for further experiments.

Synthesis of hybrid CD/CNT catalysts

The CNTs were purified by refluxing in a mixture of HNO_3/H_2SO_4 (1 : 3) for 6 h prior to use. The suspension was diluted fivefold in deionized water and filtered under vacuum, and then rinsed extensively with water until the pH was in the range of 5–6. Subsequently, the treated CNTs (tCNTs) were dried at 50 °C under vacuum for 3 h, and stored in a desiccator for subsequent experiments. Hybrid CD/CNT composites were prepared using a simple wet chemical approach. Briefly, 1 mL of a CD solution was added to 20 mL of the treated CNTs solution (0.25 mg mL^{-1}) and ultrasonicated for 2 h. The dispersed mixture was heated under reflux at 100 °C for 1 h. After cooling to room temperature, the suspensions were centrifuged and washed with water, then dried at 50 °C under vacuum overnight. Subsequently, all samples were placed individually at the central segment of a long quartz tube furnace, and the heating rate was increased to 800 °C at 5 °C min^{-1} for 2 h under N_2 gas. The furnace was then cooled to room temperature, and the samples were stored until needed. The resulting products were

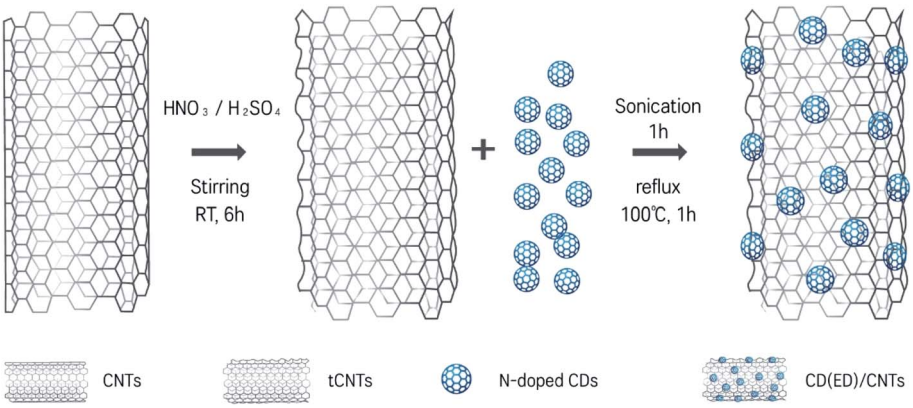

Fig. 1 Schematic diagram for the preparation of CD(ED)/CNT composites.

labeled CD(EG)/CNT, CD(EA)/CNT, and CD(ED)/CNT, respectively.

Electrochemical measurements

All electrochemical measurements were conducted using a standard three-electrode system at room temperature in a 0.1 M KOH solution, which was purged with high purity N_2 or O_2 for at least 20 min before each measurement. A saturated calomel electrode (SCE), Pt wire, and glassy carbon (GC) were used as the reference, counter, and working electrodes, respectively. All potentials were converted to the reversible hydrogen electrode (RHE) scale using the Nernst equation. The electrodes used were wet-polished with 0.05–0.3 μm aluminum slurries on a microcloth, and rinsed and sonicated in distilled water for five min to remove the residual aluminum from the electrode surface. Typically, 2 mg of each prepared catalyst was dispersed ultrasonically in 1.0 mL H_2O. Subsequently, 15 μL of the suspension was dropped onto the GC surface and dried at room temperature under vacuum. For electrochemical ORR measurements, cyclic voltammetry (CV) was performed with a CHI 601 (CH Instruments) within a potential range between 0.2 to 1.2 V (*vs.* RHE) in an O_2-saturated and N_2-saturated 0.1 M KOH at a scan rate of 50 mV s^{-1}. A CHI 705E bipotentiostat and a rotating ring-disk

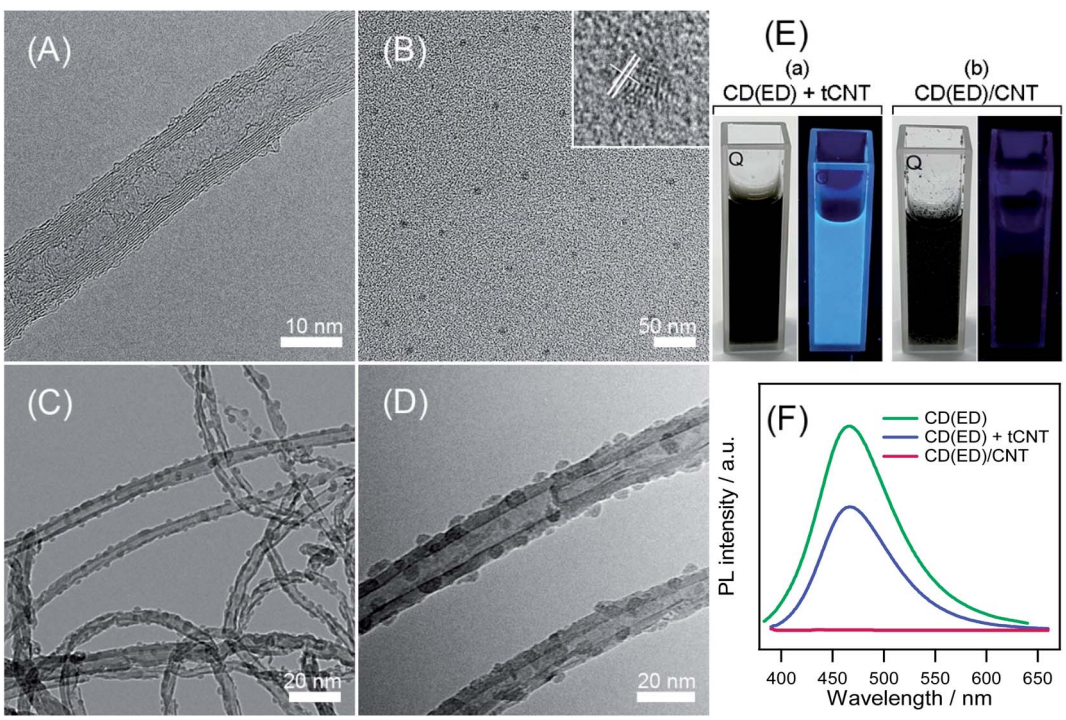

Fig. 2 TEM images of (A) tCNT, (B) N-doped CD(ED), and CD(ED)/CNT at (C) low-magnification and (D) high magnification. (E) Photos of (a) CD(ED) + tCNT and (b) CD(ED)/CNT suspensions under normal light (left) and UV light at 365 nm (right). (F) PL spectra of CD(ED), CD(ED) + tCNT, and CD(ED)/CNT, respectively.

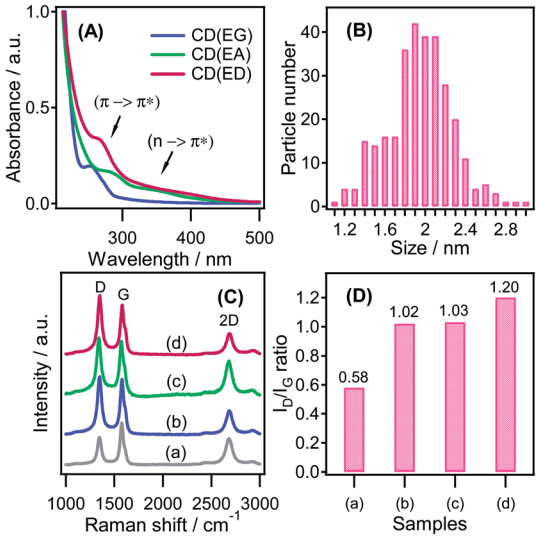

Fig. 3 (A) Absorption spectra of CDs, (B) particle size distribution histogram of CD(ED) determined from the TEM images. (C) Raman spectra and (D) I_D/I_G ratios of (a) tCNTs, (b) CD(EG)/CNT, (c) CD(EA)/CNT, and (d) CD(ED)/CNT.

electrode system (RRDE-3A, ALS Inc.) were also used for linear sweep voltammetry within a potential range between 0.2 to 1.1 V (*vs.* RHE) at a scan rate of 10 mV s^{-1} and rotating speeds ranging from 400 to 3600 rpm. A GC disk (3.0 mm diameter, 0.071 cm^2) and a rotating GC disk-platinum ring electrode (4.0 mm diameter, 0.126 cm^2) were used as the working electrode for the CV and RRDE experiments, respectively.

Results and discussion

Three types of CDs (*i.e.*, CD(EG), CD(EA) and CD(ED)) were synthesized by a general polyol process, offering a low cost, easy to use, and highly adaptable method for a broad range of system. The mechanism for the formation of CDs involves the carbonization of its constituents such as organic precursors (EG, EA, and ED solutions). The CD/CNT catalysts were prepared using a simple wet chemical method with three different CDs. The hybrid catalysts with different CD contents were labeled CD(EG)/CNT, CD(EA)/CNT, and CD(ED)/CNT, respectively. Of these, N-doped CD(ED) was introduced evenly onto the sidewalls of the CNTs, forming a new carbon hybrid lineage, such as CD(ED)/CNT. Fig. 1 presents detailed descriptions of the synthetic process. The procedure was performed in two steps: (1) pretreatment of CNTs with a mixture of HNO_3/H_2SO_4 to form defects and oxidized surfaces of CNTs, and (2) combination of CDs and CNTs to prepare the CD/CNT hybrids. Indeed, a stable suspension of CD(ED)/CNT hybrids can be obtained easily using a simple reflux method of a mixture of CNT and N-doped CD(ED). Although the origin of this hybrid structure is unclear, the π-conjugated multiple aromatic regions of CDs can interact with the sidewalls of CNTs through a π-stacking interaction.[37] Moreover, the existence of N-doped

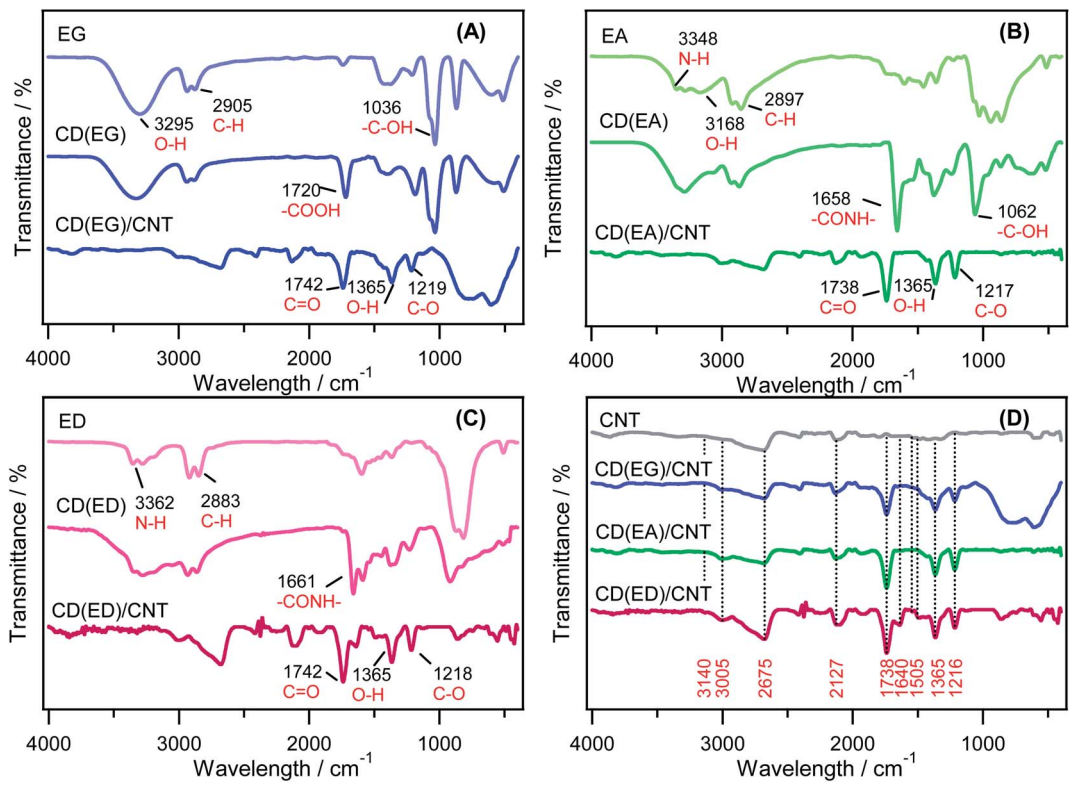

Fig. 4 FTIR spectra of CDs and CD/CNT. CDs were obtained by three-different carbon sources: (A) ethylene glycol (EG), (B) ethanolamine (EA), and (C) ethylenediamine (ED). Panel (D) compares all three CD/CNT hybrids and original CNT.

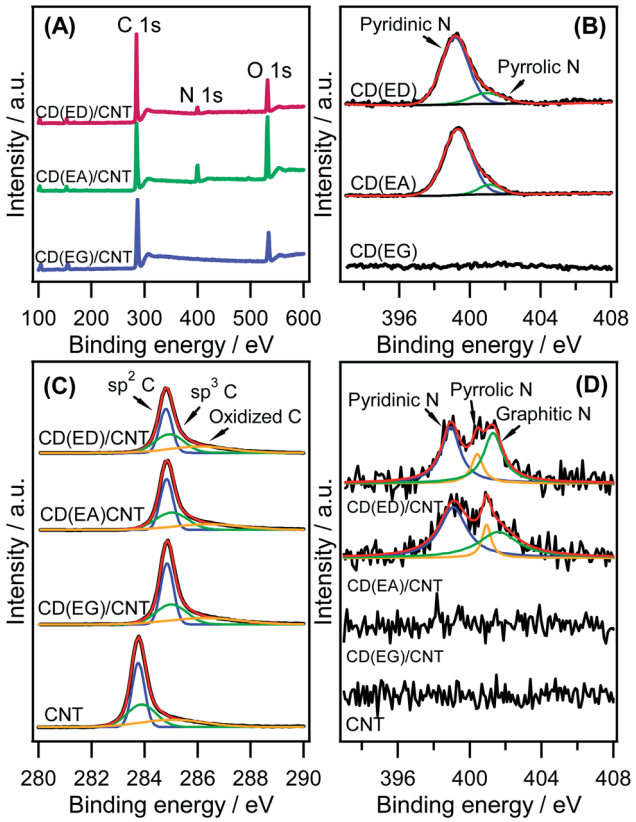

Fig. 5 Deconvoluted XPS spectra of CDs and CDs/CNT: survey (A) and N 1s (B) spectra of CD(EG), CD(EA), and CD(ED), respectively; C 1s (C) and N 1s (D) spectra of CD(EG)/CNT, CD(EA)/CNT, and CD(ED)/CNT, respectively.

CDs leads to crosslinking reactions between the amine groups of CDs and carboxylic functional groups generated during the acid treatment of the CNTs. On the other hand, CD(EA)/CNT did not introduce CDs on CNT walls as highly as CD(ED)/CNT (Fig. S1†). The primary reason is that the CD(EA)s do not provide enough amine functional groups to attach to the CNT surface at a high density. In particular, the combination of CD(EG) and CNTs to form hybrid structures was difficult under the same experimental conditions (Fig. S1†).

The use of strong oxidizing agents to generate carboxylic acid groups or carboxylated fractions on the surface of CNTs is one of the widely used strategic approaches to increase the water compatibility and binding functionality with other research purposes.[47] Fig. 2A presents the HR-TEM image after oxidizing the surface by pretreating CNTs in a mixture of HNO_3/H_2SO_4 (1 : 3) for 6 h. Compared to the smooth sidewall of un-treated CNTs (Fig. S2†), HR-TEM of the tCNT lines revealed an uneven and bumpy surface, presumably due to the formation of defects and carboxylation in the pretreatment process. On the other hand, to propose an all-carbon hybrid structure, a synthetic method of scalable CDs was developed through a wet chemical reaction of each carbon source (EG, EA, and ED) in the presence of H_2O_2 as an oxidizing agent. This method had many advantages, including gram-scale production, uniform particle sizes, excellent stability, economical approach, and simple synthetic route. TEM showed that the N-doped CD(ED)s were well-dispersed with a uniform size distribution (mean diameter of CDs was 5.8 ± 0.5 nm) (Fig. 2B). The inset at the top right revealed a well-resolved lattice structure with a *d*-spacing of 3.20, which matched the lattice spacing of graphite. Fig. 2C and D depict low- and high-magnification TEM images of the CD(ED)/CNT hybrid. N-doped CDs were anchored on the sidewalls of CNT through reflux.

The luminescence characteristics before and after the hybridization of CD(ED)s and CNTs were examined. The mixed solution of CD(ED)s and CNTs showed similar luminescence characteristics to that of CD(ED)s. In contrast, the photochemical properties of the hybrid catalyst, in which the two carbon materials were bonded, disappeared under UV light at 365 nm excitation (Fig. 2E). Although the origin of this phenomenon is unclear, it might have come from the effects of emissive trap sites on their hybrid surface because the CD(ED)s are bonded chemically, not physically, to the CNT surface.[34] Fig. 2F shows the photoluminescence (PL) spectra of the three different samples before and after hybridization. The emission maximum in the PL spectra of the mixture (CD(ED)s + CNTs) remained unchanged with the peak position around 467 nm compared to the CD(ED)s sample. On the other hand, such emission was not observed for the CD(ED)/CNT because of the formation of the hybrid. This result provides further evidence that CD(ED)s had been decorated over the walls of CNTs.

Fig. 3A shows that the as-synthesized CDs showed two typical peaks at the absorption spectra of the three CDs in an aqueous medium, corresponding to the excitation wavelengths of the π–π* transition (250–280 nm) of the aromatic ring structure and the n–π* transition (~350 nm) of the C=O or N=N group, respectively. This is a similar characteristic of heteroatom-substitutional doping in carbon materials.[48] In this observation, all three CDs emitted strong blue light luminescence in aqueous solutions (Fig. S3†), while the fluorescence intensity of the CDs increased in the order CD(EG) < CD(EA) < CD(ED) corresponding to the N-doping degree of CDs. Fig. S4† displayed the typical excitation-dependent PL behavior of all as-synthesized CDs aqueous solution, similar to the previously reported CDs.[49–51] The emission peak shifted gradually to a longer wavelength with increasing excitation wavelength. The intense PL of the CD(EG) dispersion appeared at 415 nm and 457 nm upon excitation at 320 nm, while excitation maxima of both CD(EA) and CD(ED) were 380 nm and emission maxima were 467 nm and 471 nm, respectively. The PL emission peak at 457 nm was much stronger than that of the peak at 415 nm, revealing the blue emission. Fig. 3B presents the particle size distributions of the representative CD(ED); the average particle size was 1.95 nm ± 0.32 ($n = 50$).

Fig. 3C shows the Raman spectra of all the as-obtained samples. The three main peaks at ~1350 cm^{-1}, ~1580 cm^{-1}, and ~2687 cm^{-1} correspond to the D, G, and 2D bands of these samples, respectively. The 2D peaks of the CD(ED)/CNT were up-shifted to 2686.8 cm^{-1}, compared to that of the pristine CNTs peak at 2681.8 cm^{-1}, suggesting that N-doped CDs were effectively introduced onto the CNT surface. The degree of the defect and disorder levels can be confirmed by the intensity of

the D to G ratio (I_D/I_G) (Fig. 3D). The I_D/I_G of the CD(EG)/CNT ($I_D/I_G = 1.02$), CD(EA)/CNT ($I_D/I_G = 1.03$), and CD(ED)/CNT ($I_D/I_G = 1.20$) were more intense than that of the CNTs ($I_D/I_G = 0.58$), suggesting the highest defect level in the carbon hybrid for the CD(ED)/CNT. This showed that the defect could greatly enhance the adsorption of oxygen molecules on the hybrid carbon, resulting in higher catalytic activity.

Surface functional groups on the CD precursors, CDs, and CD/CNT hybrids were determined by FTIR spectroscopy (Fig. 4). The measurement results for the EG and EA solutions confirmed the presence of –OH groups at ~3295 cm^{-1}. On the other hand, the ED solution confirmed that only the –NH groups exist, as expected from the structure. An analysis of individual CDs solution showed that the –OH groups were present in all samples. In contrast, NH functional groups were observed on the CD surface of the CD(EA) and CD(ED) solutions. CD/CNT hybrids synthesized from CD(EG), CD(EA), and CD(ED) precursors were functionalized with C=O, O–H, and C–O groups, as evidenced by peaks at 1738 cm^{-1}, 1365 cm^{-1}, and 1216 cm^{-1}, respectively (Fig. 4D).[52,53] The N–H banding vibration from CD(ED)/CNT was observed at 1640 cm^{-1} representing N-doped CD/CNT hybrid formation. This band was not observed clearly at CD(EG)/CNT and CD(EA)/CNT. Moreover, the IR absorption bands at 1505 cm^{-1} were assigned to the N–O stretching vibration derived from the CD(ED)/CNT prepared *via* a surface oxidation-assisted chemical bonding procedure. Indeed, the FTIR spectrum of the N-doped hybrid, CD(ED)/CNT, is different from that observed in the solutions of CNT, CD(EG)/CNT, and CD(EA)/CNT.

The chemical composition and surface oxidation state of the CDs and CD/CNT hybrids were investigated by XPS. N-doped CDs, such as CD(EA) and CD(ED), were prepared using a series of N-containing bases, such as ethanolamine and ethylenediamine. As shown in Fig. 5A, the XPS survey spectra revealed nitrogen concentrations of 0.0, 1.8, and 2.1 at% in CD(EG)/CNT, CD(EA)/CNT, and CD(ED)/CNT, respectively. These results showed somewhat lower N contents than that the reported for N-doped carbon (N contents: 2.9–4.8 at%).[54,55] The main reason is that N-doping processes were not performed for the entire hybrid carbon, and CDs containing N atoms were synthesized preferentially and bonded to the CNTs backbone. Two distinct components centered at 399.3 and 401.9 eV in the N 1s spectra (Fig. 5B) revealed the presence of pyridinic N and pyrrolic N in the CD(EA) and CD(ED). No such components were found in the CD(EG) sample. The C 1s spectrum of CNTs was observed at 283.8 eV, while the peaks of the high energy shifting of CD/CNT hybrids were found at 284.8 eV, corresponding to the introduction of heteroatoms such as O and N (Fig. 5C). Since the electronegativity of O and N is higher than that of base C in CNTs, the electron density around carbon in CNTs decreases and the binding energy increases. The asymmetric tail towards the higher binding energy at 285.8 eV can be explained in two ways: (1) the contribution of both C–O/C–N and C–OH functionalities; and (2) high concentration of sp^2 carbon, but no extended delocalized electrons (≥290.0 eV), were observed in all samples. This suggests that the CDs and CNT hybrids are not related to the interaction of the emitted photoelectrons and π electrons.[56] The N 1s spectra from 398 to 403 eV (Fig. 5D) were

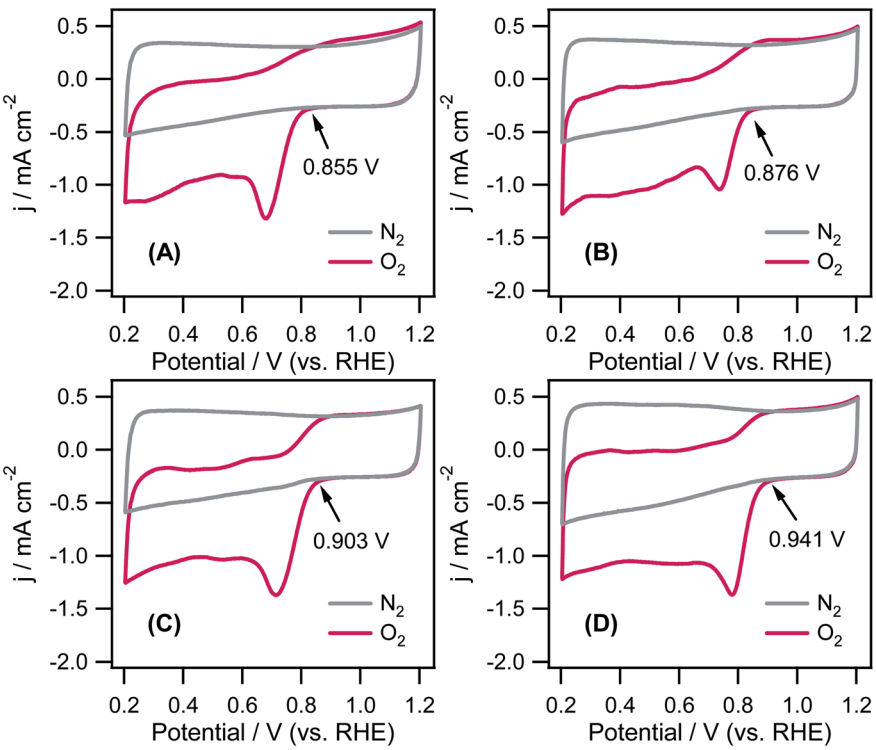

Fig. 6 CVs of (A) tCNTs, (B) CD(EG)/CNT, (C) CD(EA)/CNT, and (D) CD(ED)/CNT in O_2-saturated and N_2-saturated 0.1 M KOH at 50 mV s^{-1}. The arrows indicate onset potential.

deconvoluted into three peaks, which were associated with the contribution of pyridinic N (399.1 eV), pyrrolic N (400.3 eV), and graphitic N (401.4 eV), indicating the successful doping of a nitrogen atom into the CD(ED)/CNTs and CD(EA)/CNTs. Indeed, the pyridinic N and pyrrolic N were generated during carbonization process, while the graphitic N in carbon frameworks was mainly formed after a post-treatment at high temperature.[57] Such N dopings may endow CD(ED)/CNTs superior properties for further catalysis applications because they can act as active catalytic sites.[58] On the other hand, this peak was not observed in the CNT and CD(EG)/CNT samples.

The ORR activity of the CD/CNT hybrids was examined by cyclic voltammetry (CV) and linear sweep voltammetry (LSV) using a rotating-ring disk electrode (RRDE) in a 0.1 M KOH solution saturated with O_2 at room temperature. Fig. 6 presents the CV traces of CNT and three different CD/CNT hybrids in alkaline solutions saturated with O_2 (purple) or N_2 (gray); Table 1 lists the results. For all samples, strong reduction peak currents were observed at 0.65–0.95 V (*vs.* RHE) in an O_2 saturated environment after the ORR began. These peaks disappeared when the electrolyte solution was purged with N_2, indicating that this peak corresponds to a decrease in O_2. Considering the ORR onset potential (E_{on}) and cathodic peak potential (E_{pc}), the overall catalytic activity for the ORR on the catalysts increased in the order of CNT (E_{on} = 0.855 V *vs.* RHE) < CD(EG)/CNT (E_{on} = 0.876 V *vs.* RHE) < CD(EA)/CNT (E_{on} = 0.903 V *vs.* RHE) < CD(ED)/CNT (E_{on} = 0.941 V *vs.* RHE). This suggests that an increased N-dopant concentration with a concomitant with a change in the active sites may change the mode of oxygen adsorption on the catalyst surface, resulting in enhanced ORR performance.

To understand the electrocatalytic ORR performance of the catalysts further, the RRDE technique was used in an O_2-saturated 0.1 M KOH solution at a rate of 10 mV s^{-1} at different rotation speeds (400–3600 rpm). A commercial Pt/C

Table 1 ORR catalytic properties of CD/CNT hybrids

Catalysts	E_{pc}[a] (V *vs.* RHE)	E_{on}[a] (V *vs.* RHE)	Tafel slopes (mV dec^{-1})	C_{dl} (mF cm^{-2})
CNT	0.680	0.855	−49.4	6.6
CD(EG)/CNT	0.740	0.876	−51.4	7.7
CD(EA)/CNT	0.714	0.903	−55.4	13.4
CD(ED)/CNT	0.780	0.941	−60.9	16.9
Pt/C			−79.8	

[a] Measured by CV for CD/CNT catalysts in O_2 saturated 0.1 M KOH solution (Fig. 6).

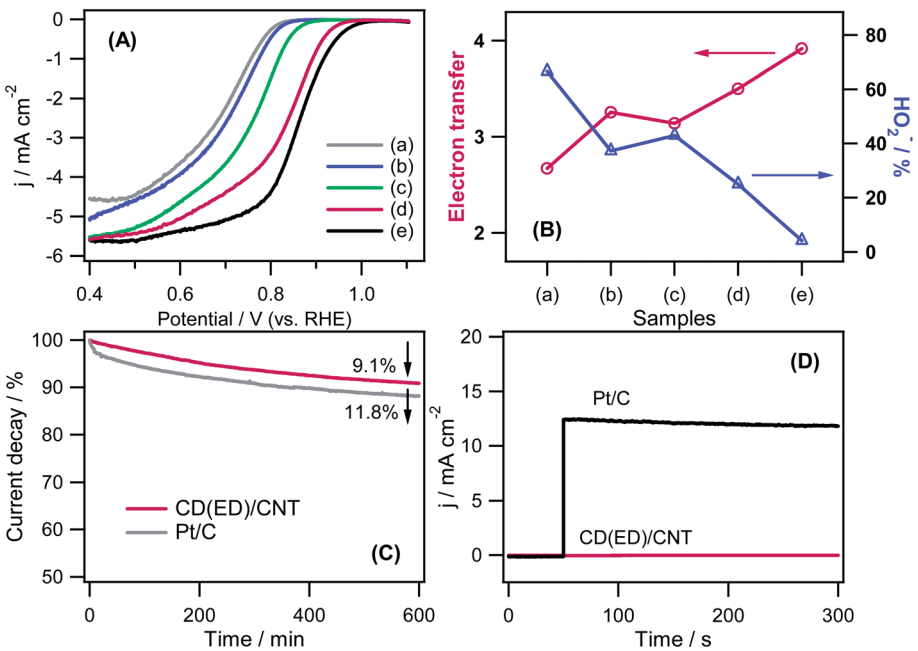

Fig. 7 (A) RRDE in O_2-saturated 0.1 M KOH solution at a rotation rate of 1600 rpm and a scan rate of 10 mV s^{-1}. (B) Diagram of the number of electrons transferred and percentages of HO_2^- generation at the disk electrode obtained from RRDE studies. (C) RDE chronoamperometric responses in O_2-saturated 0.1 M KOH solution at a rotation rate of 400 rpm for >10 h. (D) Chronoamperometric responses in an N_2-saturated 0.1 M KOH solution with the addition of 1.0 M methanol at 50 s. The samples correspond to (a) tCNTs, (b) CD(EG)/CNT, (c) CD(EA)/CNT, (d) CD(ED)/CNT, and (e) Pt/C, respectively.

catalyst was used for comparison. The onset potential shown in the RRDE in Fig. 7A is consistent with the CV results in Fig. 6. Among the carbon-based catalysts used in this study, CD(ED)/CNT exhibited the best ORR performance in terms of E_{on}, half-wave potentials ($E_{1/2}$), and current density. Commercially available Pt/C had positive potentials by ΔE_{on} = +0.040 V (E_{on} for Pt/C − E_{on} for CD(ED)/CNT) and $\Delta E_{1/2}$ = +0.026 V ($E_{1/2}$ for Pt/C − $E_{1/2}$ for CD(ED)/CNT) compared to CD(ED)/CNT. The relative catalytic activity was inferior to the commercial Pt/C, but the ORR catalytic activity was good compared to all carbon hybrids. A quantitative estimation of the electron transfer number (n) per dioxygen molecule involved in the ORR and peroxide formation by two-electron reduction of O_2 was estimated through the disk (I_d) and ring (I_r) currents: $n = 4 \times (I_d/(I_d + I_r/N))$ and HO_2^- (%) = $200 \times \{(I_r/N)/(I_d + I_r/N)\}$, where N is the collection efficiency.[21] As shown in Fig. 7B, the n value of CD(ED)/CNT for the ORR was ~3.5, and the yield of peroxide was 24.9% at +0.4 V (*vs.* RHE). Fig. 7C shows the durability test for the CD(ED)/CNT and Pt/C. Although all carbon catalysts generally exhibited lower durability than the novel metals-based nanostructures in RDE measurements, the observed durability of the CD(ED)/CNT (~9.1% decay over 10 h) was superior to the high-performance Pt/C (~11.8% decay over 10 h) catalyst. The methanol tolerances of CD(ED)/CNT and Pt/C were also determined from the chronoamperometric responses performed in N_2-saturated 0.1 M KOH solution with the addition of 1.0 M methanol at 50 s (Fig. 7D). The CD(ED)/CNT electrode exhibited a high methanol tolerance compared to the Pt/C due to suppression of the methanol oxidation reaction. On the other hand, a sudden and large anodic current density on Pt/C indicated Pt/C to have poor methanol selectivity. The overall results showed that the ORR catalytic activity of CD(ED)/CNT was greater than that of commercial Pt/C in terms of the stability and methanol tolerance.

Fig. 8A presents Tafel plots of various catalysts within the mixed kinetic-diffusion (j_k) region of the LSV curves, as shown in Fig. 7A. The Tafel slopes of CNTs, CD(EG)/CNT, CD(EA)/CNT, and CD(ED)/CNT toward the ORR were −49.4, −51.4, −55.4, and −60.9 mV dec^{-1}, respectively, which showed that CD(ED)/CNT exhibits an ideal Tafel slope at a low overpotential under alkaline conditions.[59] The results indicate the fast electron transfer rate-determining step of CD(ED)/CNT toward the ORR. Pt/C also exhibited similar behavior: a Tafel slope of −79.8 mV dec^{-1} at a low overpotential and shifts to >100 mV dec^{-1} with increasing overpotential. The electrochemical double-layer capacitance (C_{dl}) is another vital parameter to estimate the ORR activity of a catalyst. According to the non-faradaic area of CVs (Fig. S5†), the difference in $\Delta j = j_a - j_c$ at 1.00 V (*vs.* RHE) as a function of the scan rates was obtained because Δj is directly proportional to the active surface area.[60] As shown in Fig. 8B, the C_{dl} sequence of all catalysts was CNTs (6.6 mF cm^{-2}) < CD(EG)/CNT (7.7 mF cm^{-2}) < CD(EA)/CNT (13.4 mF cm^{-2}) < CD(ED)/CNT (16.9 mF cm^{-2}), which is in accordance with the high active surface of the highly decorated CDs on the CNT walls. These results suggest that an electrochemically active surface area depends strongly on the C_{dl}. Table 1 lists the ORR kinetic parameters, such as E_{pc} (V *vs.* RHE) for the ORR, E_{on}, Tafel slopes, and C_{dl}.

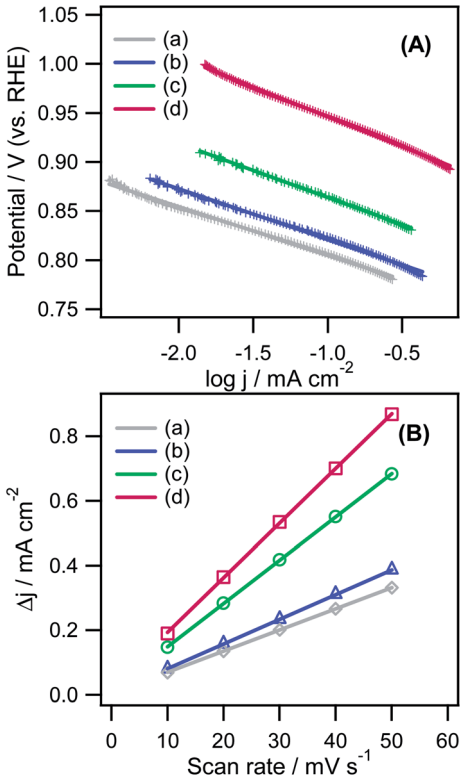

Fig. 8 (A) Tafel plots within the mixed kinetic-diffusion region of RRDE curves at 1600 rpm (B) scan rate dependence of the current densities for determining the electrochemical double-layer capacitance measured by CVs in the non-faradaic region of 0.9–1.1 V (*vs.* RHE). The samples correspond to (a) tCNTs, (b) CD(EG)/CNT, (c) CD(EA)/CNT, and (d) CD(ED)/CNT, respectively.

Conclusions

This paper proposed a facile and scalable synthesis of an all-carbon hybrid structure as an efficient alternative catalyst for the ORR in fuel cells. A scalable and stable suspension of the CD(ED)/CNT hybrid was obtained using a simple reflux method of a mixture of tCNT and N-doped CD(ED). In particular, a comparison of the CD(EG)/CNT and CD(EA)/CNT composites showed that the combination strategy of CD(ED) and CNT allowed the easy formation of a hybrid structure. Benefiting from structural advantages, the CD(ED)/CNT catalysts exhibited superior ORR performance compared to other composites and even surpassed the commercial Pt/C catalyst in terms of the Tafel slope and durability. The enhanced performance of the CD(ED)/CNT hybrid was attributed to the N-doped CD(ED)/CNT hybrid structure providing more active edges and defect sites, which play an important role in the electrocatalytic performance of the ORR. This study presented a novel all-carbon hybrid catalyst consisting of N-doped CDs and tCNT and provided new insight into the ORR performance.

Conflicts of interest

There are no conflicts to declare.

Acknowledgements

This research was supported by the Daegu University Research Grant, 2019.

References

1 C. Sealy, The problem with platinum, *Mater. Today*, 2008, **11**, 65–68.
2 M. Shao, Q. Chang, J.-P. Dodelet and R. Chenitz, Recent advances in electrocatalysts for oxygen reduction reaction, *Chem. Rev.*, 2016, **116**, 3594–3657.
3 Q. Tan, T. Qu, C.-Y. Shu, Y. Liu, Y. He, W. Zhai, S.-W. Guo, L. Liu and Y.-N. Liu, High-performance polymer fiber membrane based direct methanol fuel cell system with non-platinum catalysts, *ACS Sustainable Chem. Eng.*, 2019, **7**, 17145–17153.
4 L. Dai, Y. Xue, L. Qu, H.-J. Choi and J.-B. Baek, Metal-free catalysts for oxygen reduction reaction, *Chem. Rev.*, 2015, **115**, 4823–4892.
5 P. Y. You and S. K. Kamarudin, Recent progress of carbonaceous materials in fuel cell applications: an overview, *Chem. Eng. J.*, 2017, **309**, 489–502.
6 X. Liu and L. Dai, Carbon-based metal-free catalysts, *Nat. Rev. Mater.*, 2016, **1**, 16064.
7 R. Paul, F. Du, L. Dai, Y. Ding, Z. L. Wang, F. Wei and A. Roy, 3D heteroatom-doped carbon nanomaterials as multifunctional metal-free catalysts for integrated energy devices, *Adv. Mater.*, 2019, **31**, 1805598.
8 S. Agnoli and M. Favaro, Doping graphene with boron: a review of synthesis methods, physicochemical characterization, and emerging applications, *J. Mater. Chem. A*, 2016, **4**, 5002–5025.
9 L. Wang, H. Dong, Z. Guo, L. Zhang, T. Hou and Y. Li, Potential application of novel boron-doped graphene nanoribbon as oxygen reduction reaction catalyst, *J. Phys. Chem. C*, 2016, **120**, 17427–17434.
10 N. Yang, X. Zheng, L. Li, J. Li and Z. Wei, Influence of phosphorus configuration on electronic structure and oxygen reduction reactions of phosphorus-doped graphene, *J. Phys. Chem. C*, 2017, **121**, 19321–19328.
11 Z. Xiao, X. Huang, L. Xu, D. Yan, J. Huo and S. Wang, Edge-selectively phosphorus-doped few-layer graphene as an efficient metal-free electrocatalyst for the oxygen evolution reaction, *Chem. Commun.*, 2016, **52**, 13008–13011.
12 J. Fu, S. Wang, Z. Wang, K. Liu, H. Li, H. Liu, J. Hu, X. Xu, H. Li and M. Liu, Graphitic carbon nitride based single-atom photocatalysts, *Front. Phys.*, 2020, **15**, 33201.
13 M. Kaur, M. Kaur and V. K. Sharma, Nitrogen-doped graphene and graphene quantum dots: a review onsynthesis and applications in energy, sensors and environment, *Adv. Colloid Interface Sci.*, 2018, **259**, 44–64.
14 R. Mo, D. Rooney, K. Sun and H. Y. Yang, 3D nitrogen-doped graphene foam with encapsulated germanium/nitrogen-doped graphene yolk–shell nanoarchitecture for high-performance flexible Li-ion battery, *Nat. Commun.*, 2017, **8**, 13949.
15 K. Share, A. P. Cohn, R. Carter, B. Rogers and C. L. Pint, Role of nitrogen-doped graphene for improved high-capacity potassium ion battery anodes, *ACS Nano*, 2016, **10**, 9738–9744.
16 Z. Xing, Z. Ju, Y. Zhao, J. Wan, Y. Zhu, Y. Qiang and Y. Qian, One-pot hydrothermal synthesis of nitrogen-doped graphene as high-performance anode materials for lithium ion batteries, *Sci. Rep.*, 2016, **6**, 26146.
17 H. Xu, L. Ma and Z. Jin, Nitrogen-doped graphene: synthesis, characterizations and energy applications, *J. Energy Chem.*, 2018, **27**, 146–160.
18 T. H. Han, D. Mohapatra, N. Mahato, S. Parida, J. H. Shim, A. T. N. Nguyen, V. Q. Nguyen, M. H. Cho and J.-J. Shim, Effect of nitrogen doping on the catalytic activity of carbon nano-onions for the oxygen reduction reaction in microbial fuel cells, *J. Ind. Eng. Chem.*, 2020, **81**, 269–277.
19 H. Jiang, J. Gu, X. Zheng, M. Liu, X. Qiu, L. Wang, W. Li, Z. Chen, X. Ji and J. Li, Defect-rich and ultrathin N doped carbon nanosheets as advanced trifunctional metal-free electrocatalysts for the ORR, OER and HER, *Energy Environ. Sci.*, 2019, **12**, 322–333.
20 S. Kubendhiran, N. Karikalan, S.-M. Chen, P. Sundaresan and R. Karthik, Synergistic activity of single crystalline bismuth sulfide and sulfur doped graphene towards the electrocatalysis of tryptophan, *J. Catal.*, 2018, **367**, 252–263.
21 R. Zhang, J. R. Adsetts, Y. Nie, X. Sun and Z. Ding, Electrochemiluminescence of nitrogen- and sulfur-doped graphene quantum dots, *Carbon*, 2018, **129**, 45–53.
22 J. Yu, Y. Guo, S. Miao, M. Ni, W. Zhou and Z. Shao, Spherical ruthenium disulfide-sulfur-doped graphene composite as an efficient hydrogen evolution electrocatalyst, *ACS Appl. Mater. Interfaces*, 2018, **10**, 34098–34107.
23 J. Lee, S. Noh, N. D. Pham and J. H. Shim, Top-down synthesis of S-doped graphene nanosheets by electrochemical exfoliation of graphite: metal-free bifunctional catalysts for oxygen reduction and evolution reactions, *Electrochim. Acta*, 2019, **313**, 1–9.
24 J. Cao, Y. Hu, L. Chen, J. Xu and Z. Chen, Nitrogen-doped carbon quantum dot/graphene hybrid nanocomposite as an efficient catalyst support for the oxygen reduction reaction, *Int. J. Hydrogen Energy*, 2017, **42**, 2931–2942.
25 K. Chen, K. Liu, P. An, H. Li, Y. Lin, J. Hu, C. Jia, J. Fu, H. Li, H. Liu, Z. Lin, W. Li, J. Li, Y.-R. Lu, T.-S. Chan, N. Zhang and M. Liu, Iron phthalocyanine with coordination induced electronic localization to boost oxygen reduction reaction, *Nat. Commun.*, 2020, **11**, 4173.
26 L. Li and T. Dong, Photoluminescence tuning in carbon dots: surface passivation or/and functionalization, heteroatom doping, *J. Mater. Chem. C*, 2018, **6**, 7944–7970.
27 S.-T. Yang, X. Wang, H. Wang, F. Lu, P. G. Luo, L. Cao, M. J. Meziani, J.-H. Liu, Y. Liu, M. Chen, Y. Huang and Y.-P. Sun, Carbon dots as nontoxic and high-performance

fluorescence imaging agents, *J. Phys. Chem. C*, 2009, **113**, 18110–18114.

28 W. Ghann, V. Sharma, H. Kang, F. Karim, B. Richards, S. M. Mobin, J. Uddin, M. M. Rahman, F. Hossain, H. Kabir and N. Uddin, The synthesis and characterization of carbon dots and their application in dye sensitized solar cell, *Int. J. Hydrogen Energy*, 2019, **44**, 14580–14587.

29 C. Hu, M. Li, J. Qiu and Y.-P. Sun, Design and fabrication of carbon dots for energy conversion and storage, *Chem. Soc. Rev.*, 2019, **48**, 2315–2337.

30 T. Feng, Q. Zeng, S. Lu, X. Yan, J. Liu, S. Tao, M. Yang and B. Yang, Color-tunable carbon dots possessing solid-state emission for full-color light-emitting diodes applications, *ACS Photonics*, 2018, **5**, 502–510.

31 S. D. Hettiarachchi, R. M. Graham, K. J. Mintz, Y. Zhou, S. Vanni, Z. Peng and R. M. Leblanc, Triple conjugated carbon dots as a nano-drug delivery model for glioblastoma brain tumors, *Nanoscale*, 2019, **11**, 6192–6205.

32 W. Yang, H. Zhang, J. Lai, X. Peng, Y. Hu, W. Gu and L. Ye, Carbon dots with red-shifted photoluminescence by fluorine doping for optical bio-imaging, *Carbon*, 2018, **128**, 78–85.

33 B. Wu, G. Zhu, A. Dufresne and N. Lin, Fluorescent aerogels based on chemical crosslinking between nanocellulose and carbon dots for optical sensor, *ACS Appl. Mater. Interfaces*, 2019, **11**, 16048–16058.

34 Y. Wang and A. Hu, Carbon quantum dots: synthesis, properties and applications, *J. Mater. Chem. C*, 2014, **2**, 6921–6939.

35 H. Liu, Q. Zhao, J. Liu, X. Ma, Y. Rao, X. Shao, Z. Li, W. Wu, H. Ning and M. Wu, Synergistically enhanced activity of nitrogen-doped carbon dots/graphene composites for oxygen reduction reaction, *Appl. Surf. Sci.*, 2017, **423**, 909–916.

36 J. Han, G. Huang, Z. Wang, Z. Lu, J. Du, H. Kashani and M. Chen, Low-Temperature Carbide-Mediated Growth of Bicontinuous Nitrogen-Doped Mesoporous Graphene as an Efficient Oxygen Reduction Electrocatalyst, *Adv. Mater.*, 2018, **30**, 1803588.

37 M. Zhao, J. Zhang, H. Xiao, T. Hu, J. Jia and H. Wu, Facile *in situ* synthesis of a carbon quantum dot/graphene heterostructure as an efficient metal-free electrocatalyst for overall water splitting, *Chem. Commun.*, 2019, **55**, 1635–1638.

38 H. Feng, P. Xie, S. Xue, L. Li, X. Hou, Z. Liu, D. Wu, L. Wang and P. K. Chu, Synthesis of three-dimensional porous reduced graphene oxide hydrogel/carbon dots for high-performance supercapacitor, *J. Electroanal. Chem.*, 2018, **808**, 321–328.

39 H. Jin, H. Huang, Y. He, X. Feng, S. Wang, L. Dai and J. Wang, Graphene quantum dots supported by graphene nanoribbons with ultrahigh electrocatalytic performance for oxygen reduction, *J. Am. Chem. Soc.*, 2015, **137**, 7588–7591.

40 J.-J. Zhang, Z.-B. Wang, C. Li, L. Zhao, J. Liu, L.-M. Zhang and D.-M. Gu, Multiwall-carbon nanotube modified by N-doped carbon quantum dots as Pt catalyst support for methanol electrooxidation, *J. Power Sources*, 2015, **289**, 63–70.

41 X. Zhou, Z. Tian, J. Li, H. Ruan, Y. Ma, Z. Yang and Y. Qu, Synergistically enhanced activity of graphene quantum dot/multi-walled carbon nanotube composites as metal-free catalysts for oxygen reduction reaction, *Nanoscale*, 2014, **6**, 2603–2607.

42 V. Georgakilas, D. Gournis, V. Tzitzios, L. Pasquato, D. M. Guldi and M. Prato, Decorating carbon nanotubes with metal or semiconductor nanoparticles, *J. Mater. Chem.*, 2007, **17**, 2679–2694.

43 H. G. Shiraz and M. G. Shiraz, Palladium nanoparticle and decorated carbon nanotube for electrochemical hydrogen storage, *Int. J. Hydrogen Energy*, 2017, **42**, 11528–11533.

44 J. Saleem, S. K. Safdar Hossain, A. Al-Ahmed, A. Rahman, G. McKay and M. M. Hossain, Evaluation of Pd nanoparticle-decorated CeO_2–MWCNT nanocomposite as an electrocatalyst for formic acid fuel cells, *J. Electron. Mater.*, 2018, **47**, 2277–2289.

45 R. Akbarzadeh, M. Ghaedi, S. Nasiri Kokhdan and D. Vashaee, Remarkably improved electrochemical hydrogen storage by multi-walled carbon nanotubes decorated with nanoporous bimetallic Fe–Ag/TiO_2 nanoparticles, *Dalton Trans.*, 2019, **48**, 898–907.

46 C. Yang, Q. Jiang, W. Li, H. He, L. Yang, Z. Lu and H. Huang, Ultrafine Pt nanoparticle-decorated 3D hybrid architectures built from reduced graphene oxide and MXene nanosheets for methanol oxidation, *Chem. Mater.*, 2019, **31**, 9277–9287.

47 A. R. Deline, B. P. Frank, C. L. Smith, L. R. Sigmon, A. N. Wallace, M. J. Gallagher, D. G. Goodwin, D. P. Durkin and D. H. Fairbrother, Influence of Oxygen-Containing Functional Groups on the Environmental Properties, Transformations, and Toxicity of Carbon Nanotubes, *Chem. Rev.*, 2020, **120**, 11651–11697.

48 P. Wu, W. Li, Q. Wu, Y. Liu and S. Liu, Hydrothermal synthesis of nitrogen-doped carbon quantum dots from microcrystalline cellulose for the detection of Fe^{3+} ions in an acidic environment, *RSC Adv.*, 2017, **7**, 44144–44153.

49 Z. Ding, F. Li, J. Wen, X. Wang and R. Sun, Gram-scale synthesis of single-crystalline graphene quantum dots derived from lignin biomass, *Green Chem.*, 2018, **20**, 1383–1390.

50 X. Ma, S. Li, V. Hessel, L. Lin, S. Meskers and F. Gallucci, Synthesis of luminescent carbon quantum dots by microplasma process, *Chem. Eng. Process.*, 2019, **140**, 29–35.

51 X. Wei, L. Li, J. Liu, L. Yu, H. Li, F. Cheng, X. Yi, J. He and B. Li, Green Synthesis of Fluorescent Carbon Dots from Gynostemma for Bioimaging and Antioxidant in Zebrafish, *ACS Appl. Mater. Interfaces*, 2019, **11**, 9832–9840.

52 X. Zhang, J. Wang, J. Liu, J. Wu, H. Chen and H. Bi, Design and preparation of a ternary composite of graphene oxide/carbon dots/polypyrrole for supercapacitor application: importance and unique role of carbon dots, *Carbon*, 2017, **115**, 134–146.

53 X. Dong, Y. Su, H. Geng, Z. Li, C. Yang, X. Li and Y. Zhang, Fast one-step synthesis of N-doped carbon dots by pyrolyzing ethanolamine, *J. Mater. Chem. C*, 2014, **2**, 7477–7481.

54 K. Gong, F. Du, Z. Xia, M. Durstock and L. Dai, Nitrogen-doped carbon nanotube arrays with high electrocatalytic activity for oxygen reduction, *Science*, 2009, **323**, 760.

55 K. N. Chaudhari, M. Y. Song and J.-S. Yu, Transforming Hair into Heteroatom-Doped Carbon with High Surface Area, *Small*, 2014, **10**, 2625–2636.

56 J. V. Rojas, M. Toro-Gonzalez, M. C. Molina-Higgins and C. E. Castano, Facile radiolytic synthesis of ruthenium nanoparticles on graphene oxide and carbon nanotubes, *Mater. Sci. Eng., B*, 2016, **205**, 28–35.

57 T. Sharifi, G. Hu, X. Jia and T. Wågberg, Formation of active sites for oxygen reduction reactions by transformation of nitrogen functionalities in nitrogen-doped carbon nanotubes, *ACS Nano*, 2012, **6**, 8904–8912.

58 N. P. Subramanian, X. Li, V. Nallathambi, S. P. Kumaraguru, H. Colon-Mercado, G. Wu, J.-W. Lee and B. N. Popov, Nitrogen-modified carbon-based catalysts for oxygen reduction reaction in polymer electrolyte membrane fuel cells, *J. Power Sources*, 2009, **188**, 38–44.

59 T. Shinagawa, A. T. Garcia-Esparza and K. Takanabe, Insight on Tafel slopes from a microkinetic analysis of aqueous electrocatalysis for energy conversion, *Sci. Rep.*, 2015, **5**, 13801.

60 A. T. N. Nguyen and J. H. Shim, Facile one-step synthesis of Ir–Pd bimetallic alloy networks as efficient bifunctional catalysts for oxygen reduction and oxygen evolution reactions, *J. Electroanal. Chem.*, 2018, **827**, 120–127.